



Research papers

Latent heat thermal energy storage in a shell-tube: A wavy partial layer of metal foam over tubes

Mehdi Ghalambaz^{a,*}, Mutabe Aljaghtham^b, Ali J. Chamkha^c, Mehdi Fteiti^d,
Abdelkader Abdullah^{b,e}

^a Institute of Research and Development, Duy Tan University, Da Nang 550000, Viet Nam

^b Department of Mechanical Engineering, College of Engineering in Al-Kharj, Prince Sattam Bin Abdulaziz University, Al-Kharj 11942, Saudi Arabia

^c Faculty of Engineering, Kuwait College of Science and Technology, Doha District 35004, Kuwait

^d Physics Department, Faculty of Applied Science, Umm Al-Qura University, Makkah 24381, Saudi Arabia

^e Mechanical Power Engineering Department, Faculty of Engineering, Tanta University, Tanta 31521, Egypt



ARTICLE INFO

Keywords:

Wavy metal foam layer
Latent heat thermal energy storage (LHTES)
Finite element method
Shell-tube

ABSTRACT

The melting thermal energy storage and heat transfer of paraffin wax in a storage unit was modeled in the presence of a wavy copper foam. The phase-change energy and natural convection effects were modeled using the enthalpy porosity approach. The control equations were solved using the finite element method over a structured mesh. The energy storage was simulated for the wavenumber and amplitude of the foam layer. It was found that the higher wavenumber, the shorter the charging time and better energy storage power. A lower wave magnitude was also better than a longer wave magnitude. The shortest melting time was obtained for a flat foam layer, which was 20 % better than a low wave long amplitude foam layer. The current work intends to reduce the weight of applied metal foams in thermal energy storage applications by enhancing the geometry design. Here, a wavy form layer of metal foam was used to guide the natural convection flows and also boost the heat transfer mechanism. The phase change heat transfer has not been investigated in a wavy form metal foam layer.

1. Introduction

Currently, conventional fossil fuels are the world's primary source of energy. Nonetheless, because fossil fuels are nonrenewable and threaten the environment, renewable energy sources are becoming more common. Because renewable energy sources, particularly solar and wind, are intermittent and fluctuating, efforts are being made to mitigate these shortcomings. Thermal energy storage (TES), which has been critical in the rapid growth of global economic development [1], could help solve this problem. The advancement of TES technology is hampered by a scarcity of high-performance thermal storage materials [2]. This technique uses phase change materials (PCMs) such as paraffin and fatty acids, which have good thermochemical stability, low melting temperatures, are accessible and can absorb and release a significant amount of energy at a constant temperature [3,4]. It is widely used in solar heating, building energy conservation, and waste heat recovery [5]. Using nanoparticles [6], two phase boiling [7], and fins [8] are some of recent approaches for heat transfer enhancement.

The charging and discharging performance of the TES segments

determines the overall system performance [9]. However, the thermal conductivity of most organic phase change materials is low, reducing heat transfer performance during phase change processes [10]. In recent decades, scientists have looked into ways to improve the thermal properties of heat storage materials. Encapsulation [11], the application of carbon nanotubes [12], the use of fins [13], integrating PCM with graphite [14], and the inclusion of metal foam [15] are examples of these methods. The most direct and effective way to improve the thermal properties of PCM is to improve the thermal conductivity [16]. According to previous studies, adding PCMs to porous media such as expanded graphite and metal foam (MF) can improve their thermal conductivity [17,18]. In this investigation, metal foam PCM (MFPCM) composite is considered since it offers fast heat transfer paths, is low cost, and can enhance heat transfer [19].

Recently, thin-film MFPCMs have been used to invent thermal management systems for cooling electronic components such as GPU, CPU, laptops, LCDs, and tablets [20]. Considering that PCMs can absorb relatively large quantities of heat from battery cells, Mehmet Dede and Joshi [21] used MFPCMs to create battery cells that operated at a lower

* Corresponding author.

E-mail addresses: mehdighalambaz@duytan.edu.vn, ghalambaz.mehdi@gmail.com (M. Ghalambaz).

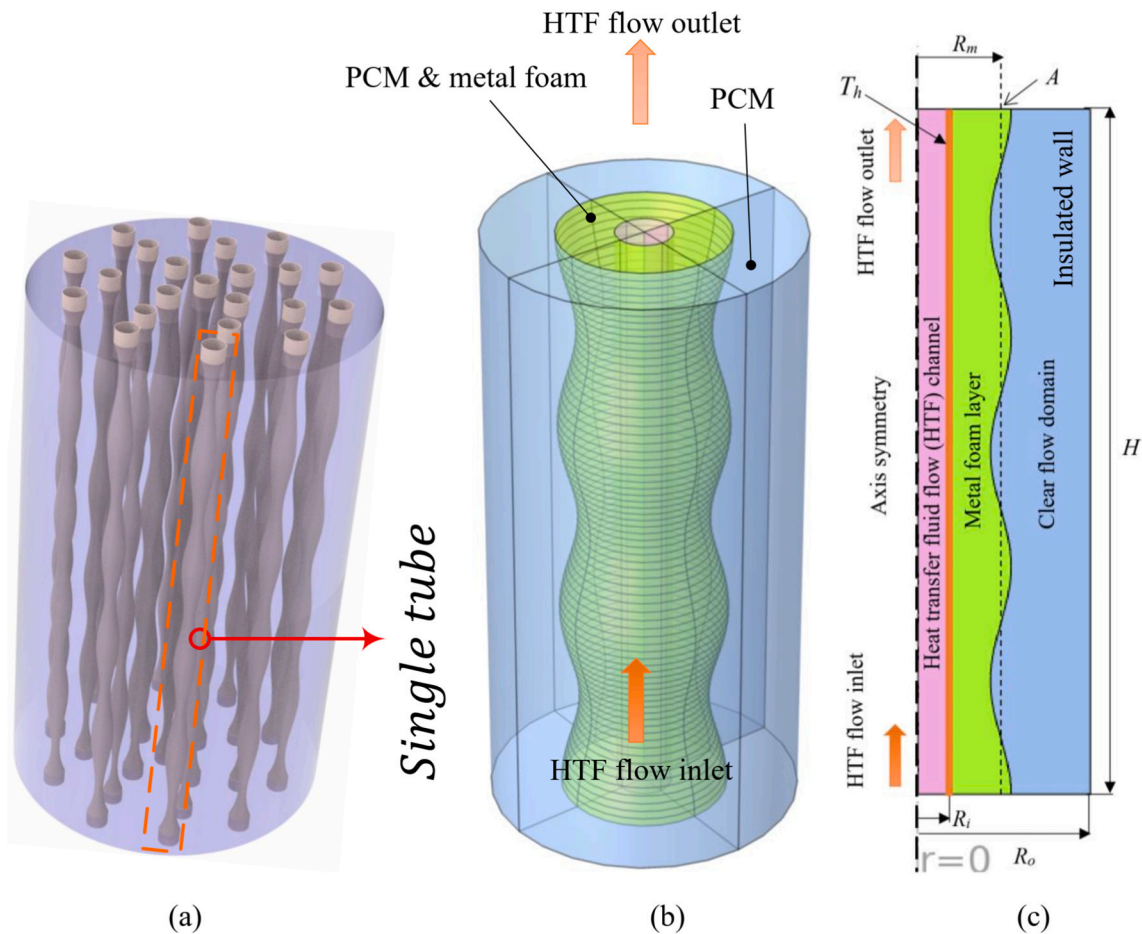


Fig. 1. A schematic view of the physical model; (a) Latent heat thermal energy storage (LHTES) unit, (b) A 3D model of a single tube with a layer of metal foam, and (c) A 2D axis-symmetric model of a single tube with a wavy layer of metal foam.

Table 1
Thermophysical properties of paraffin wax and copper [46].

Property (unit)	Copper foam	Paraffin wax
ρ_{PCM} (kgm^{-3})	8900	900
μ_l (Nsm^{-2})	N/A	0.0324
k ($\text{Wm}^{-1} \text{K}^{-1}$)	380	0.3
C_p (JkgK^{-1})	386	2300
ρ_{PCM} (kgm^{-1})	8900	900
h_f (kJkg^{-1})	N/A	148.8

temperature. The invention can increase the amount of electrical energy produced and extend battery life. The film's heat transfer has also been investigated in some recent studies [22].

The average temperature of a porous-PCM system and the temporal evolution were studied numerically by Sardari et al. [23] in a vertical container with copper foam. PCM with copper foam melted in almost 85 % less time than pure PCM. Li et al. [24] utilized numerical methods to investigate the impact acceleration had on the behavior of the copper-PCM alloy. The enhancement of natural convection produced a more sloping liquid-solid interaction with a varying temperature; additionally, melting fractions rose as acceleration increased. Using

experimental and computational techniques, Al Siyabi et al. [25] showed PCM inside a cylindrical TES with an inclined angle of 45 degrees exhibited the quickest melting rate. Using the rectangular enclosure, Punniakodi et al. [26] found that PCM melt rate was highest at a 60-degree angle of inclination. Even though the inclination angle can effectively change heat transfer for pure PCM, the inclination angle did not significantly influence the melting behavior of MFPCM. The increase in resistance due to the MF hampered free convection growth, which is why this happened [27].

Yang et al. [28] conducted visual tests to investigate the impact of a porous copper foam on heat transfer performance in a TES system. Compared to pure PCM, the optimized composite PCM could shorten the melting time by 64 %. Yao et al. [29] explored the impact of pore density as well as porosity on the heat transfer capabilities of MFPCMs by modifying the MF structural parameters. According to the findings, the thermal conductivity of MF materials is adversely related to their porosity and pore density. The less porous and dense the material, the higher its thermal conductivity. Meng et al. [30] examined the influence of copper foam porosity on the performance of TES by using numerical models. As a result, they determined that increasing the density of the copper/paraffin composite improved its thermal performance. In another study, Meng et al. [31] examined the heat transfer characteristics of a shell-and-tube TES system filled with copper foam at various compression levels. According to the study, charging/discharging times

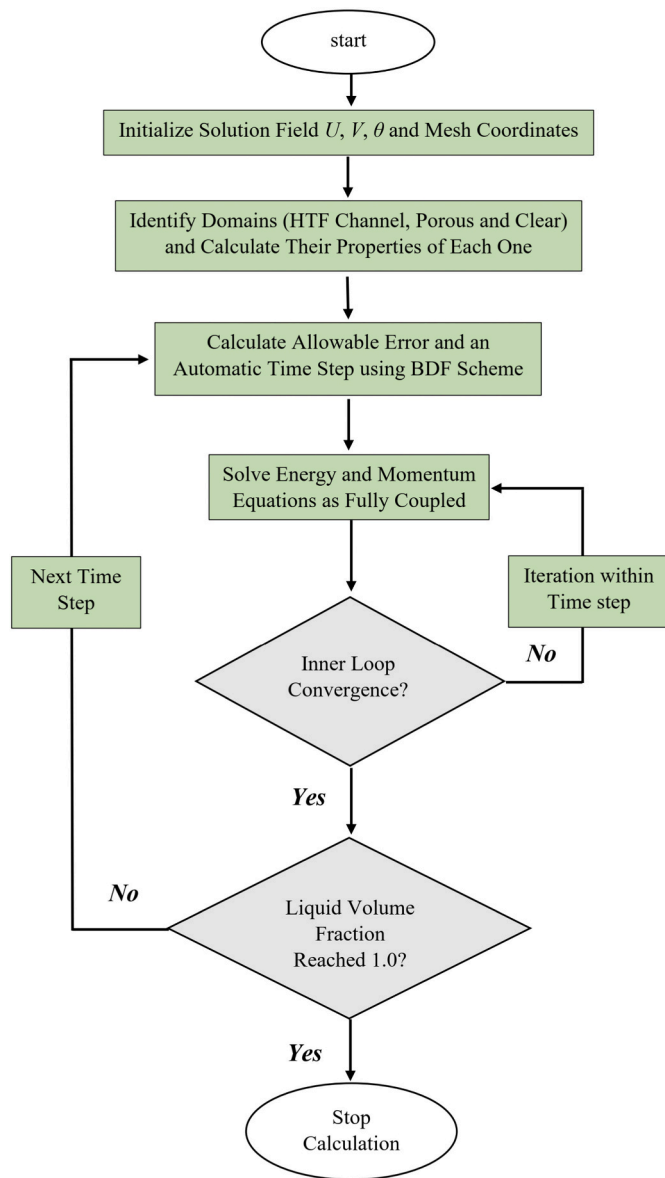


Fig. 2. The diagram of the solution method. The Computational scheme starts by initializing the filed variables over discrete domains followed by computing the closure relations.

Table 2
The adopted grids for computations for Case 4 with $A = 3$ mm and $N = 3$.

Grid name	Number of cells	Edge elements	MVF @1500s	%Err ^a
Grid I	3600	498	0.916	12.3
Grid II	4350	508	0.915	12.1
Grid III	8325	749	0.848	3.9
Grid IV	28,875	1279	0.817	0.1
Grid V	112,500	2550	0.816	-

^a %Err = $100 \times (\text{Grid} - \text{Grid V}) / \text{Grid V}$.

were reduced by 93.32 % and 97.63 % when loading volumes of 47.83 % and 100 %, respectively. In addition, the metallic framework contributed significantly to an increase in flow resistance, whereas the increased filling volume slowed the heat transfer process.

A theoretical study has been conducted by Borhani et al. [32] to examine how porous media and PCM can increase the performance of thermoelectric generators. The findings demonstrate that using a porous

medium on the thermoelectric generator’s cold side produces more power than using PCM with a porous medium on both sides. Huang et al. [33] studied the melting and heat transfer properties of an MFPCM composite in a rectangular system at various inclination degrees. MFPCM systems with varying tilt angles demonstrated varying thermal behavior and melting qualities, although MF ligaments inhibited free convection. Yu et al. [34] adapted MFPCM to cool electronic devices by modifying the porosity of the MF via directed compression. Ali [35] examined various sink configurations using nickel foam and paraffin wax to improve electronics thermal management. In hypergravity, Ding et al. [36] studied the melting properties of MFPCM composites. A key objective of this study was to determine the nature of the process involved in melting PCM in MF in hypergravity, as well as to derive design guidelines for an optimal latent heat management system.

Some recent studies utilized wavy surfaces for heat transfer improvement in latent heat thermal energy storage designs. For example, Qasem et al. [37] used an enclosure with a wavy surface to enhance heat transfer. There was a rotating cylinder in the enclosure to mix the liquid PCM. The results showed that using just one undulation could improve the heat transfer much better than four undulations. Satyender and Singh [38] utilized wavy fins in a single-pass solar air heater to enhance the heat transfer and store solar energy in PCM placed below the wavy fins. Authors reported that mounting wavy find over a PCM layer was efficient for thermal energy storage in the solar air heater. Eisapour et al. [39] utilized wavy tubes in shell-tube latent heat thermal energy storage designs. Two wavy heat pipes were placed inside the shell to enhance the energy release. The results showed that employing double heat pipes could improve energy release by more than 10 %. A straight configuration could provide a slightly better thermal performance than a wavy design. Wavy surfaces have also been used in the form of wire coils have been used in corrugated tubes as heat transfer enhancers [40].

The presence of MFs can effectively improve local thermal conductivity; however, previous studies have shown that the presence of MFs reduces free convection [41]. TES tubes packed with compressed MFs were developed by Guo et al. [36] under various compressibility ratios, and their performance compared to that of uncompressed was assessed. Based on their results, compression of MF with a proper compressive ratio resulted in a better heat transfer enhancement by increasing thermal conductivity and strengthening by free convection. A partial-filling strategy has recently been proposed to fully utilize the potential of natural convection and heat transfer enhancement [42].

As seen, the wavy surface designs have been proposed in several recent designs since they can provide extended surfaces for heat transfer between PCM and the surroundings. MF has been used as one of the effective heat transfer enhancement techniques in latent heat thermal energy storage systems. The present study aims to combine the MF with wavy designs to provide a locally enhanced layer of wavy metal foam over the heat transfer tube in a shell-tube thermal energy storage design for the first time.

2. Formulation and model description

2.1. Physical model

A schematic view of a shell-tube latent heat thermal energy storage unit is depicted in Fig. 1. As seen, a bundle of tubes is packed inside a shell enclosure. Inside, the enclosure is filled with PCM. A wavy layer of open-cell metal foam is placed over tubes in which the PCM fills the porous pores. A wavy surface has been used in structural designs since it provides an extended contact surface and high mechanical strength. Thus, the PCM-metal foam forms a composite medium with improved thermal conductivity and is expected to improve the heat transfer and reduce the melting time of PCM inside the unit.

Fig. 1(b) illustrates a single tube with a layer of metal foam and surrounding PCM. A hot heat transfer fluid enters the tube from the

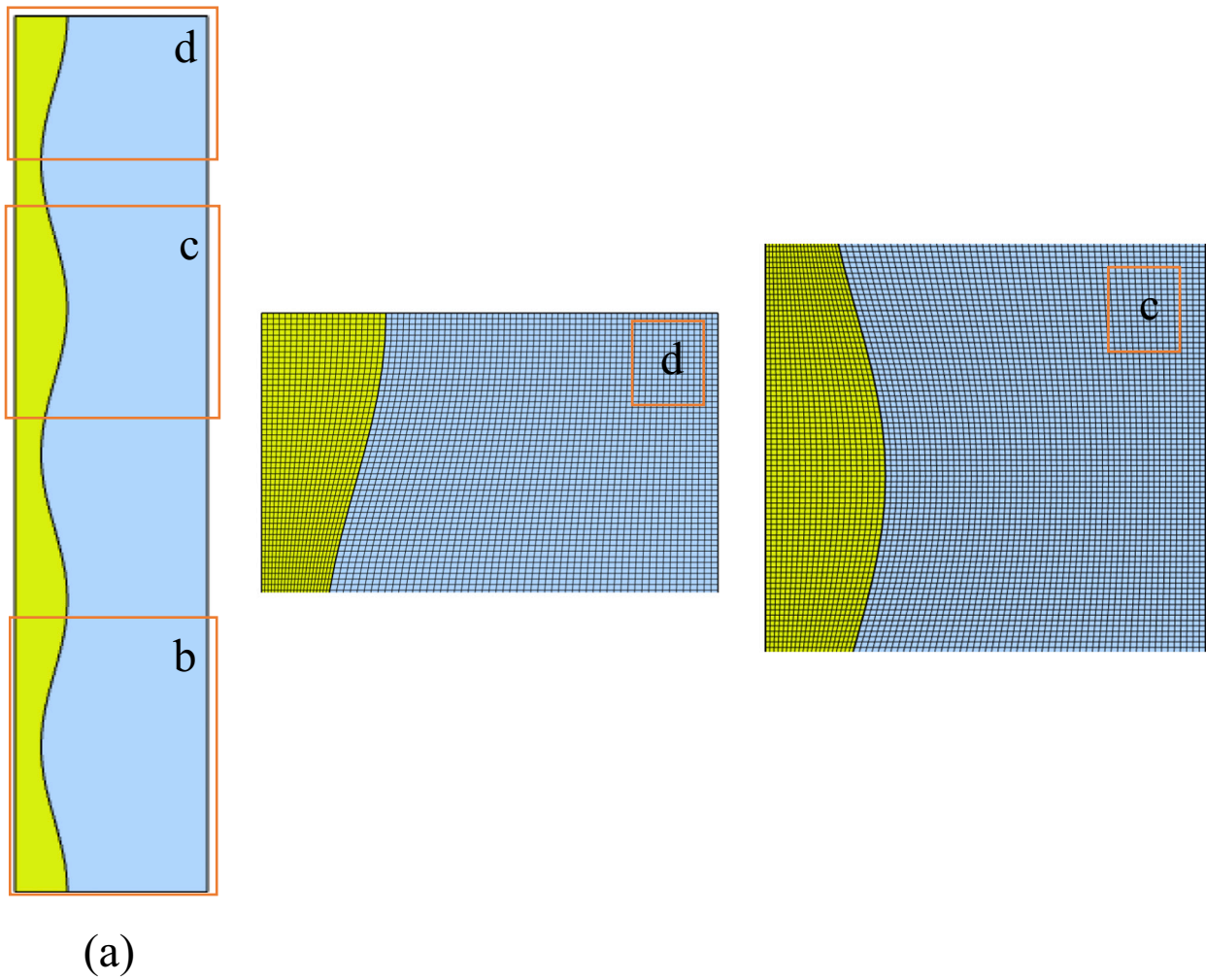


Fig. 3. Grid IV for case A = 3 mm and N = 3; (a) An overall view of model and domains, (b) Grid view at the bottom, (c) Grid view at the top, and (d) Grid view at the middle.

bottom and leaves the tube at the top. Due to the axial symmetry of the PCM, metal foam layer, and the surrounding PCM, the 3D model of the tube is modeled by a 2D axis-symmetric domain. In the beginning, the PCM inside the enclosure is at a super cold temperature T_c . Later, when the hot HTF flows inside the tube, there is a heat transfer between the HTF and the PCM inside the enclosure. The PCM absorbs heat from HTF flow and stores latent heat by phase change from solid to liquid during a melting process. Due to the natural convection, a circulation flow could occur in the liquid PCM. It is assumed that convective heat transfer due to the HTF flow is substantial, and hence, the inner surface of the tubes is at a constant hot temperature T_h . Thus, the governing equations for the present physical model are the continuity of mass, momentum, and energy, which will be addressed in the next section.

2.2. Mathematical model

The enthalpy-porosity approach was employed to model the heat transfer and natural convection in the PCM domain. Due to the presence of phase change, the heat capacity of the PCM is a function of temperature. Moreover, a sink term is added to the momentum equation to prevent fluid motion in solid PCM. The sink term induced an extremely large resistance to the fluid motion, preventing any convective heat transfer in a solid PCM domain. A Darcy source term describes the fluid flow in the metal foam domain. Thus, the momentum equation in the

porous layer can be considered as the Darcy-Brinkman model. Thus, the governing equations for the conservation of mass, momentum, and energy for the present problem can be explained by the following set of partial differential equations:

Mass conservation.

$$\frac{\partial u_i}{\partial x_i} = 0 \tag{1}$$

Momentum conservation:

$$\frac{\rho_{pcm}}{\varepsilon} \frac{\partial u_i}{\partial t} + \frac{\rho_{pcm}}{\varepsilon^2} \left(u_j \frac{\partial u_i}{\partial x_j} \right) = -\frac{\partial P}{\partial x_i} + \left[\frac{\partial}{\partial x_j} \left(\frac{\mu_{pcm}}{\varepsilon} \frac{\partial u_i}{\partial x_j} \right) \right] + f_{ext,i} \tag{2}$$

Energy conservation:

$$(\rho c_p)_{eff} \frac{\partial T}{\partial t} + (\rho c_p)_{pcm} \left(u_i \frac{\partial T}{\partial x_i} \right) = \frac{\partial}{\partial x_i} \left(k_{eff} \frac{\partial T}{\partial x_i} \right) + f_i \tag{3}$$

where $u_1 = u$ and $x_1 = x$, while $u_2 = v$, and $x_2 = y$. The thermal conductivity (k), dynamic viscosity (μ), specific heat capacity (c_p), and density (ρ) represent the physical quantities. The PCM properties and effective properties are denoted by subscripts of PCM and eff, respectively. In the momentum equation, f_{ext} represents the external forces which here is a combination of the sink term (f_{sink}) for control of velocity in solid and liquid regions, the Darcy term (f_{Darcy}), and the buoyancy

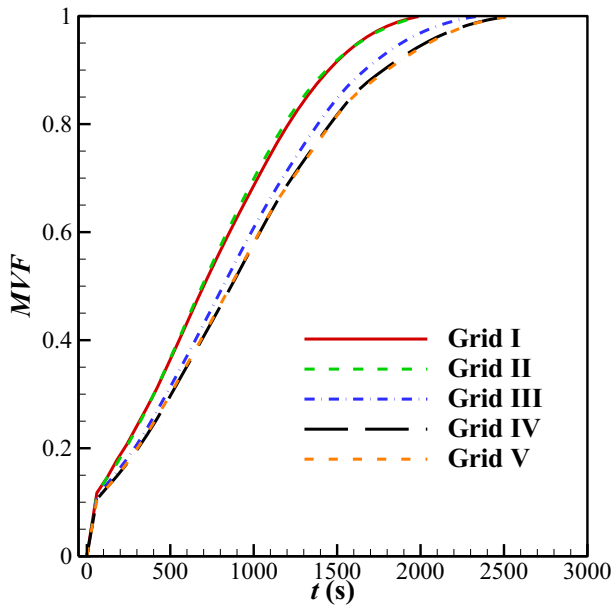


Fig. 4. Impact of the mesh size on the accuracy of the results. There is a gap between Grid size II and course and grid size III and finer. Grids IV and V are almost identical, and hence, grid IV was adopted for simulations.

force (f_b). Hence, $f_{ext} = f_{sink} + f_{Darcy} + f_b$, in which:

$$f_{sink,i} = -A_{mush} \frac{1 - 2\theta(T) + \theta^2(T)}{\lambda + \theta^3(T)} \cdot u_i, f_{Darcy,i} = -\frac{\mu_{pcm}}{\kappa} u_i, \quad (4a)$$

$$f_{b,i} = \begin{cases} 0 & i = 1 \\ g\beta_{pcm}(T - T_f)\rho_{pcm} & i = 2 \end{cases}, \quad (4b)$$

The term f_i in Eq. (3) corresponds to the variation of heat capacity due to latent heat, which can be explained by:

$$f_i = \rho_{pcm} \epsilon L_f \frac{\partial \gamma(T)}{\partial t} \quad (4c)$$

in which the latent heat of phase change (L_f), phase change temperature (T_f), and volumetric thermal expansion (β), are physical properties. Besides, the gravity constant and mushy constants are adopted as $g = 9.81 \text{ m/s}^2$, $\lambda = 0.001$, and, $A_{mush} = 10^{10} \text{ (Pa}\cdot\text{s/m}^2\text{)}$. The molten volume fraction, γ , is a function of temperature as:

$$\gamma(T) = \begin{cases} 1 & T > (T_i + \Delta T_i/2) \\ \left(\frac{T - T_i}{\Delta T_i}\right) + \frac{1}{2} & (T_i + \Delta T_i/2) < T < (T_i + \Delta T_i/2) \\ 0 & T < (T_i - \Delta T_i/2) \end{cases} \quad (5)$$

where the values of $\gamma = 1$ and zero represent the molten and solid PCM, respectively. In the clear flow domain, the porosity is unity, and the permeability is infinity, while they take the porosity and the permeability of the metal foam layer in the porous region. Thus, the porosity and permeability of the domain can be explained by the following function:

$$\epsilon = \begin{cases} \epsilon_1 & \text{metal foam} \\ 1 & \text{lear flow} \end{cases}, \text{ and } K = \begin{cases} K_1 & \text{metal foam} \\ \infty & \text{clear flow} \end{cases} \quad (6)$$

The effective heat capacity and thermal conductivity of the PCM and

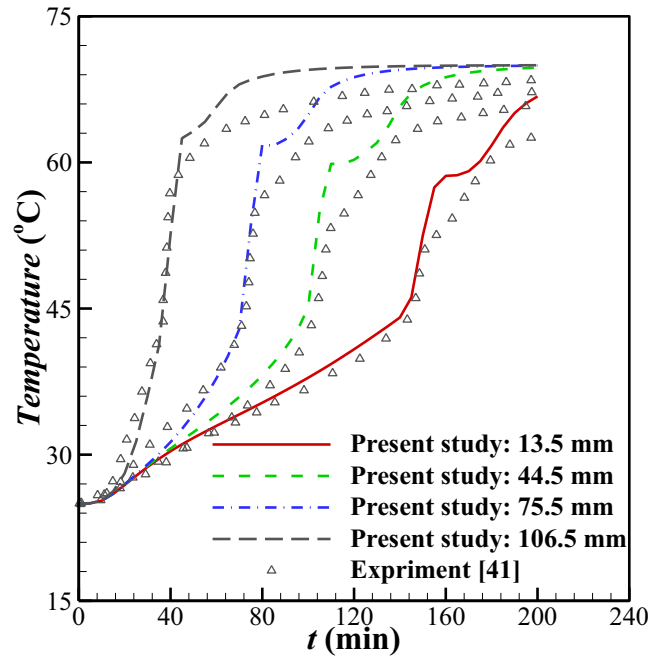


Fig. 5. The temperature distribution as a function of time in an enclosure filled with paraffin wax at four points along a vertical line at the middle plane of the enclosure. A comparison between experimental measurements of [49] and the present simulations.

metal foam are evaluated using the following relationships:

$$(\rho C_p)_{eff} = (1 - \epsilon)(\rho C_p)_{foam} + \epsilon(\rho C_p)_{pcm} \quad (7)$$

where the subscript of foam denotes the metal foam. Effective thermal conductivity is a combination of parallel and series thermal conductivity structures as [43]:

$$k_{eff} = \frac{1 - \delta}{\left(\frac{1 - \epsilon}{k_m} + \frac{\epsilon}{k_{PCM}}\right)} + \delta((1 - \epsilon)k_m + \epsilon k_{PCM}) \quad (8)$$

where $\delta = 0.35$ according to [43] which provides excellent agreement with physical measurements of [44]. The permeability of the foam layer is also computed from the below relationship [45]:

$$K = d_p^2 \frac{73 \times 10^{-5}}{(1 - \epsilon)^{0.224}} (d_i d_p^{-1})^{-1.11} \quad (9a)$$

$$(d_i d_p^{-1}) = 1.18 \left(\frac{1 - \epsilon}{3\pi}\right)^{0.5} [1 - \exp(-(1 - \epsilon)/0.04)]^{-1} \quad (9b)$$

in which $d_p = 254 \times 10^{-4} / \omega$ where $\omega = 5\text{PPI}$, and $\epsilon_1 = 0.95$. Using, Eqs. (9a) and (9b), the foam permeability was evaluated as $K = 3.8614\text{E-}7 \text{ m}^2$. The PCM is adopted as paraffin wax with a phase change

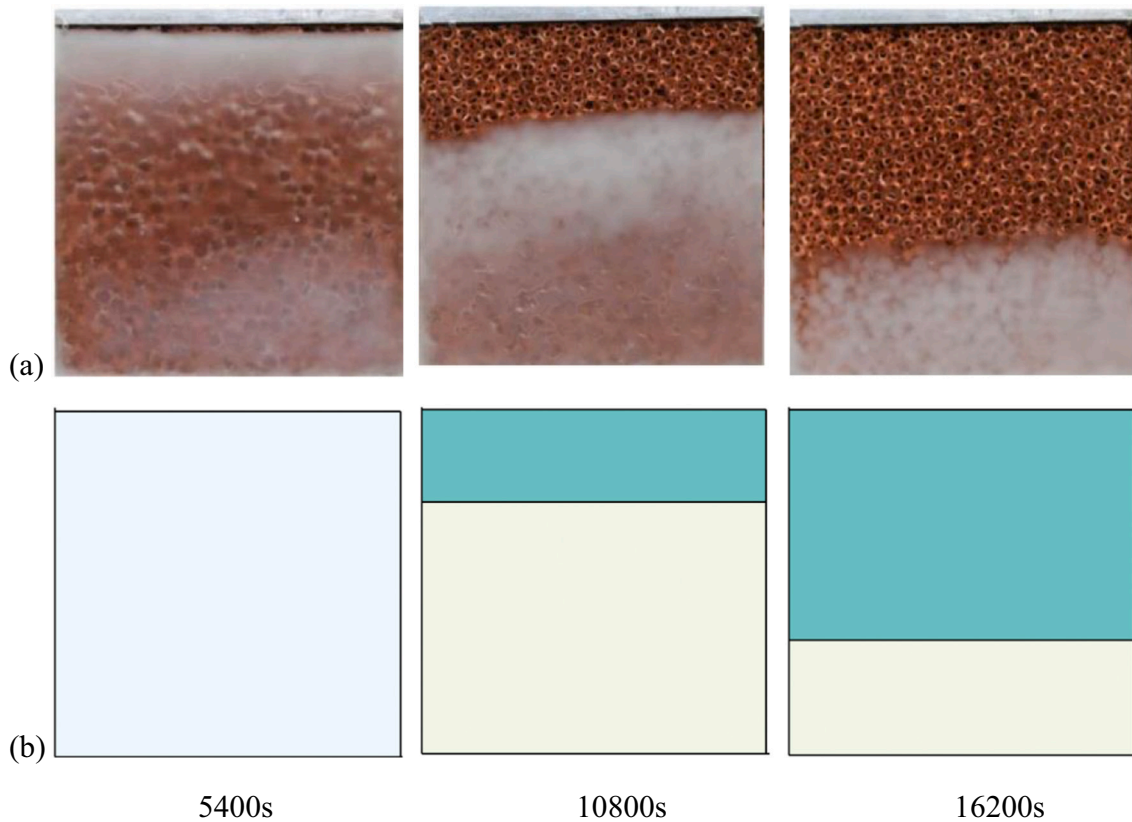


Fig. 6. Melting of composite paraffin wax -copper foam in a cavity heated from the top. The melting interface by (a) Experimental data with permission from Elsevier [46], and (b) the present simulations. A good visual agreement between the empirical context and simulation can be seen.

Table 3
The number of waves and amplitude of the investigated cases in the current.

Case	Amplitude of wave (A) mm	Number of Wave (N)
C1	3	1
C2	3	2
C3	3	3
C4	3	4
C5	3	5
C6	3	6
C7	5	1
C8	5	2
C9	5	3
C10	5	4
C11	5	5

temperature of 54 °C, which is suitable for most domestic heating applications, and the metal foam is made of copper. Moreover, the inner radius of HTF tube (R_i), the domain radius (R_o), and the porous layer base radius (R_m) are adopted as 6 mm, 50 mm, and 18 mm, respectively.

Table 1 lists the properties of the utilized material.

Considering the boundary conditions, the inner surface of the tube is at an isothermal hot temperature $T_h = 95$ °C, while the paraffin wax was initially at a super cold temperature 45 °C. The top, bottom, and perimeter surfaces of the domain are at zero heat flux. There is no slip and no permeability at the domain surfaces.

Finally, the melting volume fraction (MVF) and the energy storage (ES) were introduced as:

$$MVF = \frac{\int_V \epsilon \gamma dV}{\int_V \epsilon dV} \tag{10a}$$

where $dV = 2\pi r dr dz$ is the axis-symmetric volume element of the enclosure.

$$ST = \text{sensible energy} + \text{latent energy} \tag{10b}$$

where the sensible energy term was computed by $2\pi \int (\int_{T_c}^T (\rho C_p)_{eff} dT) r dr dz$, and the latent heat energy term was computed as $\int_V \epsilon \gamma L_f dV$.

3. Numerical method and code validation

3.1. Numerical method

The finite element method (FEM), as described in [47], was invoked to solve the governing equations for the velocity components, pressure, and temperature fields over a discretized domain. The governing equations and corresponding boundary conditions were written in the weak form and integrated over the grid elements to reach residual equations. Then, the residual equations were solved using the Newton method with a fully coupled scheme to find the unknown fields over the domain of the solution. An automatic time-step scheme [48] was also employed to keep the accuracy of the solutions within a relative error of 10^{-4} . The diagram of the solution procedure is depicted in Fig. 2. The grid check and verification of the method are discussed in the following sections.

3.2. Grid check

The influence of grid space on the accuracy of the results was checked by computing the results using several grid sizes according to Table 2. The domain of the solution was discretized using a uniform

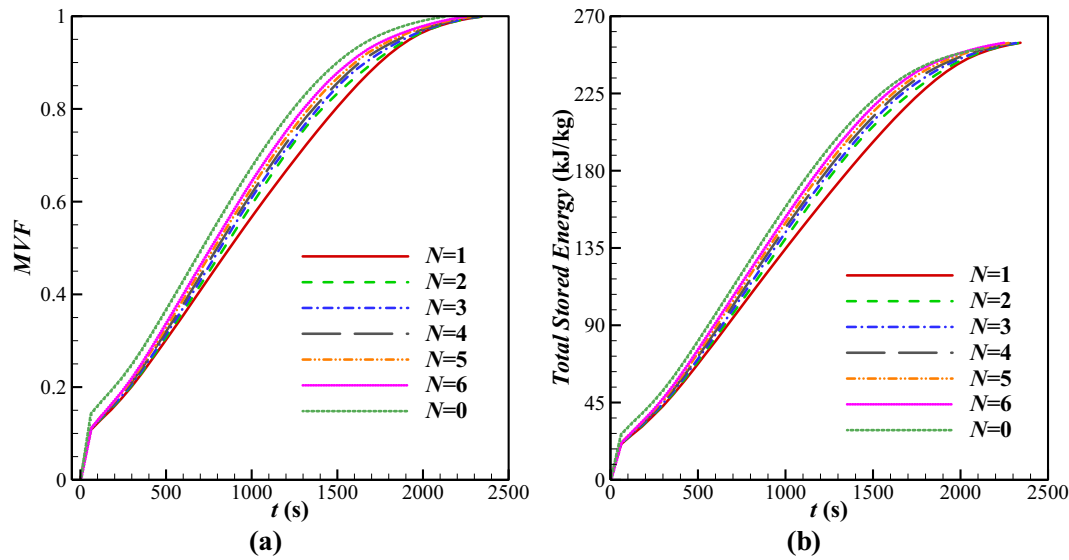


Fig. 7. Effect of wavenumber (N) parameter on; (a) Melting volume fraction, and (b) Total stored energy. The increase of wave number generally increases the thermal energy storage and melting volume fraction. Wave number $N = 1$ leads to the lowest MVF and ES.

structured grid, as depicted in Fig. 3. Table 2 shows that using a coarse grid could result in a significant error of 12 % compared to a fine grid. Moreover, the melting volume fraction, MVF, is plotted for selected grids as a function of time. This figure also shows a coarse grid could lead to a notable computational error. However, a fine grid could produce stable and accurate results. Thus, a fine grid should be used to capture the melting interface and temperature gradients adequately. Here, Grid IV with 28,875 quad cells could provide excellent accuracy, which was selected for the computations of the present study. A view of the adopted grid is shown in Fig. 4.

3.3. Verification and comparison with literature studies

The outcomes of the FEM code are compared with the available data in the literature to ensure the accuracy of the simulations. Kamkari et al. [49] examined the melting heat transfer in a rectangular cavity of 120 mm in height and 50 mm in width filled with paraffin wax. All walls were well insulated except the left vertical wall, which was isothermally heated. They placed several thermocouples inside the cavity to measure the temperature variations. The initial temperature of paraffin wax was 25 °C, while the heated wall was maintained at a hot temperature of 70 °C. Fig. 5 illustrates the comparison between the current code and the experimental data of Kamkari et al. [49]. The values in mm show the distance from the bottom on a vertical plane with a 25 mm distance from the heated wall.

Moreover, the present simulation results are compared with the experimental data [46] for melting paraffin wax in copper metal foam in an enclosure with a width and height of 100 mm. The enclosure was a cavity of size 100 mm saturated with composite PCM at an initial cold temperature of 14 °C, which was heated from the top. The melting interface was captured and reported at three time-snaps of 5400 s, 10800 s, and 16,200 s. The experimental images are compared with simulation data in Fig. 6, which confirms a good agreement.

4. Results and discussion

In the results section, the influence of the wavenumber and wave amplitude on the melting fraction and the amount of stored energy will be evaluated. Table 3 shows a summary of the simulated cases. In addition to the cases listed in the table below, a reference case, C0, was also simulated with $N = A = 0$, which represents a foam layer with no waviness. Case C0 is plotted along with the graphs for the sake of comparison. It is worth mentioning that for each fixed domain, the area of the porous region is independent of the number of the wavenumber.

Fig. 7 shows the wavenumber effect on MVF and total SE. In this figure, the time history of MVF and total SE are plotted for cases C1 to C6 and C0. As shown in Fig. 7(a), in the very first moments, the melt fraction rises sharply and then increases smoothly. This is because the metal foam-PCM layer is just next to the hot wall, and it quickly absorbs the heat from the tube. After a while, the PCM inside the metal foam melts down entirely, and then the melting process advances in the clear region. This is where MVF increases slowly. The small difference between the curves in this region is due to the natural convection effects. Increasing the number of waves accelerated the melting process between the 500 s and 1800s. A flat metal foam layer ($N = 0$) provides the highest melting rate, and foam with $N = 1$ is the worst. As the wavenumber increases, the results tend to be the case of $N = 0$. Therefore, by increasing the number of waves (assuming an infinite number of waves), it can be seen that the amplitude effect will be minimal. It is expected that the wavy design enhances the local thermal conductivity next to the HTF tube with minimal inference with later convection circulation flows. However, there is a close competition between thermal conduction enhancement and interruption of natural convection circulations. The presence of the metal foam undulations, extended to the PCM space, delays the formation of natural convection circulations.

Therefore, as seen, there is no significant difference between the results of Fig. 7 because of the close competition of two heat transfer mechanisms during the melting process. The presence of a wavy foam layer enhanced the effective thermal conductivity locally, but it also

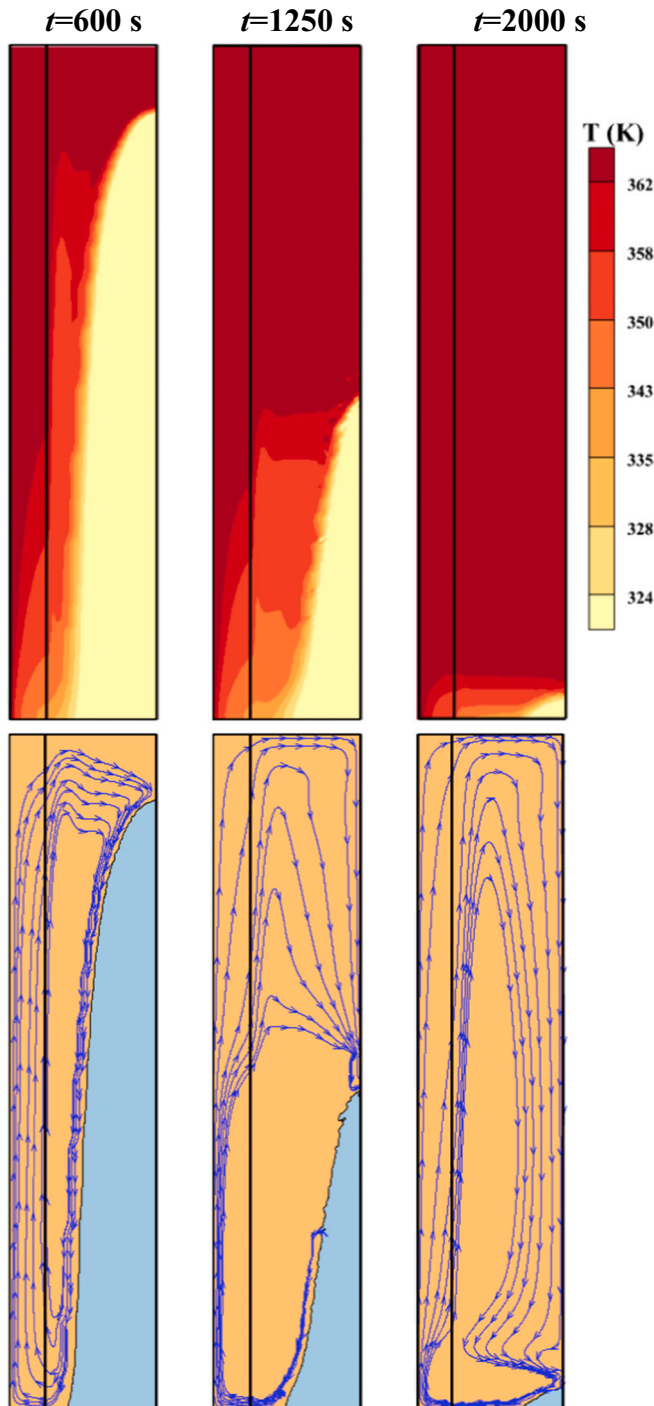


Fig. 8. (Top row) Contour of isotherm, and (Bottom row) Streamlines provided for case 0 with $N = A = 0$. The melting interface starts next to the heated wall and moves toward the insulated walls. As melting advances, the top and right regions of the enclosure enter a fully liquid state.

weakened the natural convection circulations. Thus, the change of design parameters enhances one mechanism while partially deteriorating another. As a result, the change of heat transfer characteristics by variation of design parameters is small.

In general, for each number of waves, all curves eventually reach full melting simultaneously, approximately 2300 s. Hence, the corrugated porous region, with any number of waves and even in the absence of a wave (C0 with $N = 0$), can only affect the melting fraction of the phasing

material for a certain period. However, as time advances, the distance of the melting front from the edge of the foam layer increases, and the dependency of the melting front on the foam layer decreases. A significant amount of energy storage takes place in the form of latent heat. Thus, ES curves follow almost the same pattern as the MVF. At any corresponding time, if the advance of the melting front is low, the amount of ES is also low.

Fig. 8 depicts the isotherms (first row) and the streamlines (second row) for case zero ($N = 0$). As mentioned, Case C0 indicates the model regardless of the amplitude and, consequently, the number of waves. Hence, the results for different wavenumbers and amplitude sizes will be comparable to conditions with no waves. The isotherms are in the range of 324–362 K, which is slightly above the initial temperature and next to the hot temperature. This range can adequately depict the temperature levels inside the enclosure. At the initial time ($t = 10$ min), the width of the isotherms reaches the central areas of the enclosure. Then it develops to the lower-right areas of the enclosure. Next to the full melting ($t = 2000$ s), most of the enclosure area, particularly at the top regions, reaches a temperature above 362 K, but a small region at the bottom is still in a solid-state. Next to the solid region, there is a high density of temperature lines, which shows a high-temperature gradient. As can be seen in the bottom row, there is a uniform distribution of streamlines at the foam layer while the streamlines are packed next to the solid region. Since the foam layer is uniformly heated and there is a uniform resistance to the fluid flow in the foam layer, such behavior is expected.

Figs. 9 and 10 compare the isotherms and streamlines for two cases with a wavenumber $N = 1$ (lowest wavenumber) and $N = 6$ (highest wavenumber) at three time-snaps of 600 s, 1250s, and 2000s. In 600 s and 1250s, it can be seen that the isotherms developed in the enclosure better by the increase of the wavenumber. The compression of the isotherms in 2000s shows the case $N = 6$ generally covered most of the enclosure with a hot temperature region compared to $N = 1$. The cold region at the bottom is also small for $N = 6$ compared to $N = 1$. According to **Fig. 10**, the pattern of streamlines and melting fronts in the early time ($t = 600$ s) could be notably influenced by the wavenumbers. However, the impact of wavenumber on the melting front diminishes as time advances. At $t = 600$ s and 1250, a wide gap and better-molten circulation between the heated wall and the melting front can be seen for $N = 6$ compared to $N = 1$. In general, following the results obtained in **Figs. 7 and 8**, is only significant at initial times when the melting occurs inside and next to the foam layer.

The influence of the wave amplitude on the MVF and the total ES are shown in **Fig. 11(a) to (d)**. The left and right vertical axes represent the MVF and the total ES, respectively. **Fig. 11(a)–(d)** corresponds to the wavenumbers $N = 1–4$, respectively. In all cases, the reference case, Case C0, is also plotted for the sake of comparison. As seen, the reference case C0 generally has a higher MVF and a SE than other cases at all times. Subsequently, a case with a small amplitude ($A = 3$ mm) shows a better charging characteristic than a large amplitude ($A = 5$ mm). It is important to note that there is no noticeable difference between the curves obtained for different wavenumbers. In fact, it can be seen that regardless of the number of waves, changing the amplitude value imposes almost the same effect on the melting fraction and the amount of energy stored. This is because the foam layer's contribution was limited to the enhancement of conduction heat transfer locally where the PCM is embedded in the foam. There is a natural convection dominant heat transfer mechanism in the clear region, far from the foam layer. The foam layer does not much influence this natural convection heat transfer in clear regions. The streamlines in the foam layer in **Fig. 10** denoted that the foam layer provides a uniform flow of molten PCM to the clear flow, which was not impacted by the wavy shape.

In order to evaluate the effect of wave amplitude on the isotherms and streamlines, Cases 4 and 10 were selected, and the results are reported in **Figs. 12 and 13**. As seen, by increasing the waviness amplitude to $A = 5$ mm, more severe bottlenecks are created between the edge of the foam layer and the vertical hot wall. Thus, for the case $A = 5$ mm, a

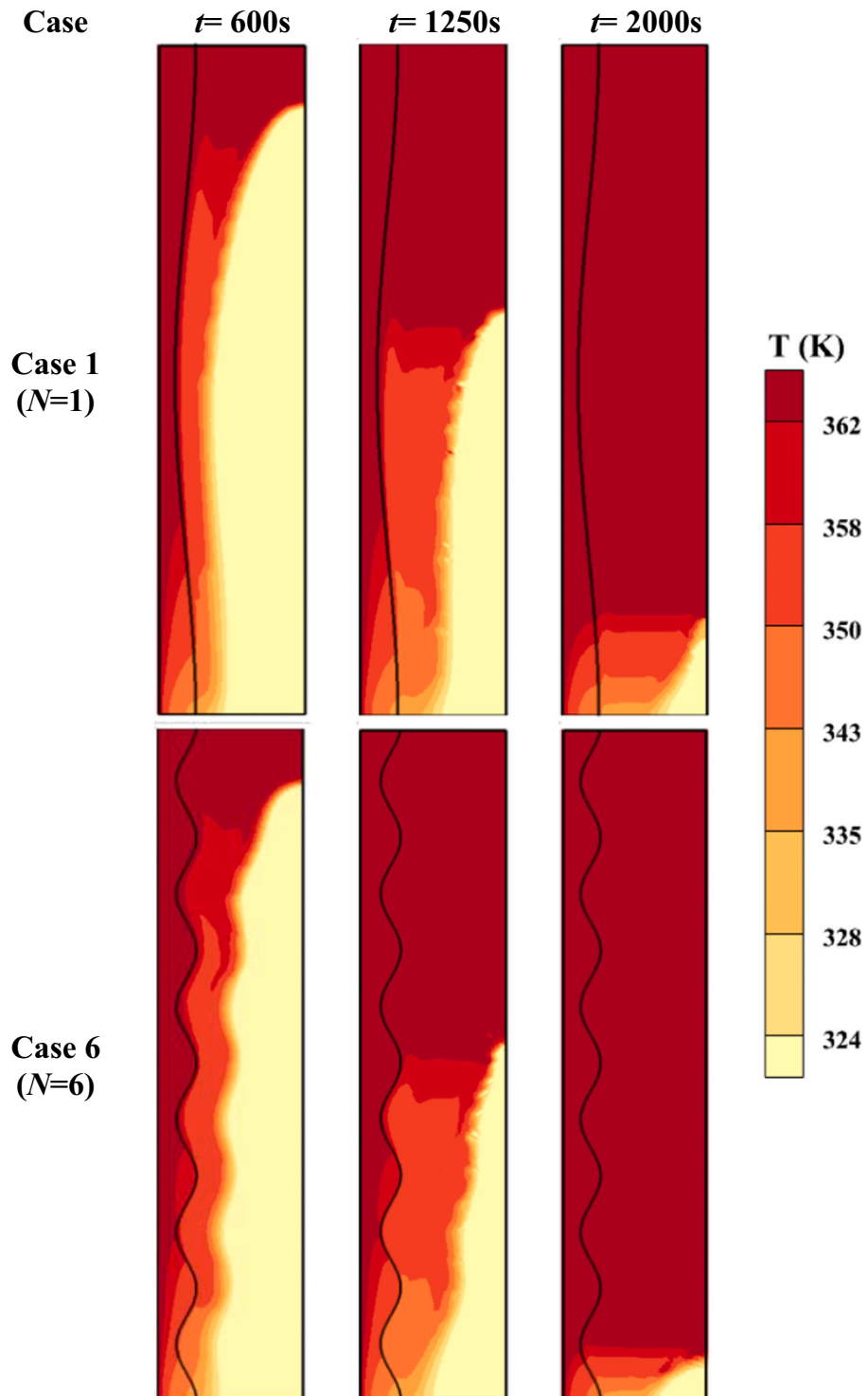


Fig. 9. Effect of wavenumber on isotherm contours; (a) Case 1 with $N = 1$, and (b) Case 6 with $N = 6$. There is a gap between the melting interface and the wavy metal foam which is mostly under the influence of the wave number.

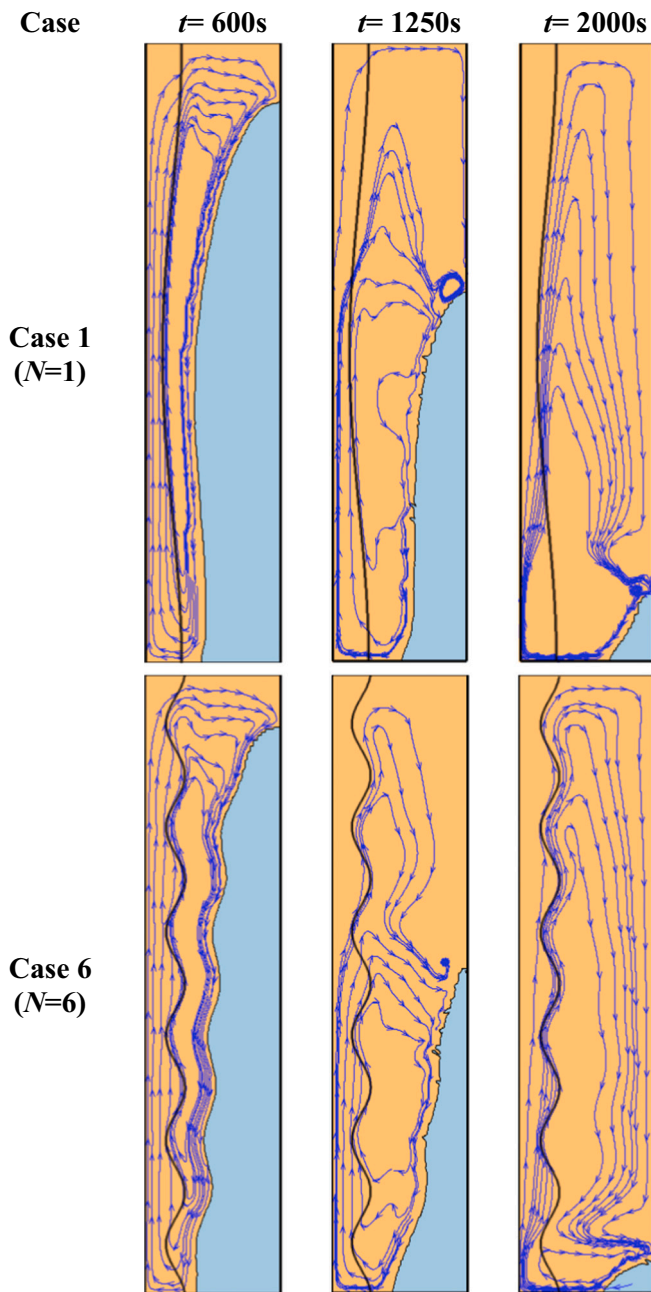


Fig. 10. Effect of wavenumber on the streamlines; (a) Case 1 with $N = 1$, and (b) Case 6 with $N = 6$. The shape of the melting front is under the direct influence of the wavy metal foam. For case $N = 6$, a wavy shape melting front can be noted. Similarly, for case $N = 1$, there is a general undulation shape in the melting front due to the shape of the metal foam.

non-uniform melting at initial times could be expected. However, attention to the results reveals that the increase of foam thickness in other locations compensates for the bottlenecks. As a result, an overall uniform temperature and melting distribution could be seen. Attention to streamlines shows that the streamlines and melting interface copies the wavy shape of the foam layer, but the amplitude of the wavy foam

cannot change the trend of the results.

The evaluation of the stored energy power at $t = 1250$ s is shown in Fig. 14. The stored energy power was computed as total ES over time. Case zero with $N = A = 0$ shows the most stored energy power, followed by case 6. The lowest stored energy power can be seen for case 7, with $N = 1$ and $A = 5$ mm. It can also be seen that from cases 1 to 6, the stored energy power can be changed smoothly by increasing the number of waves at fixed wave amplitudes. The energy storage power for case C0 was 20 % better than the reference case at $t = 1250$ s. The storage power for case 6 is only 3 % lower than the reference case at $t = 1250$ s.

5. Conclusion

The latent heat thermal charging of a shell-tube-shaped LHTES unit filled with paraffin wax PCM and enhanced by a wavy layer of copper foam was investigated. The enthalpy-porosity approach was applied to simulate the phase change in the unit. An axis-symmetric model of the tube and wavy foam layer was created and solved using the finite element method. The melting volume fraction, total stored energy, and energy storage power were plotted. The isotherm contours and streamlines were also investigated to understand the details of waviness on the energy storage behavior of the unit. The impact of foam wavenumber and amplitude on the melting volume fraction and stored energy was addressed. The most important results are as follows:

- At a constant wave amplitude, as the wavenumber increases, the melting fraction and the amount of stored energy always improve. The initial melting and final melting times are almost independent of the wavenumber. The wavenumber could smoothly change the melting front and stored energy when the melting front reached the clear flow regions.
- At a fixed wavenumber, the wave amplitude could change the MVF and SE at the intermediate stages of the charging process. The total melting time is almost independent of wave amplitude.
- The foam layer with a flat shape provides the shortest charging time. After that, the best case corresponds to the highest number of waves ($N = 6$) and smallest wave amplitude ($A = 3$ mm). Moreover, the longest storage time was obtained for the maximum amplitude and the lowest number of waves ($N = 1$ and $A = 5$ mm). The case with a flat foam layer could provide a storage energy power 20 % higher than the case with $N = 1$ and $A = 5$ mm in the middle of the charging process, i.e., $t = 1250$ s. As discussed in the introduction, the results of the present study agree well with the findings of Eisapour et al. [39] for discharging a latent heat thermal energy storage with wavy tubes and without MF.

CRediT authorship contribution statement

M. Ghalambaz: Visualization, Formal analysis, Data Curation, Software, Validation, Conceptualization, Methodology, Supervision, Writing- Original draft preparation, Writing - Review & Editing; **M. Aljaghtham:** Conceptualization, Methodology, Software, Formal analysis, Validation, Writing- Original draft preparation, Writing - Review & Editing; **A. J. Chamkha:** Methodology, Writing - Review & Editing, Investigation, Validation, Software; **M. Fteiti:** Methodology, Writing-Original draft preparation, Writing - Review & Editing, Investigation, Software; **A. Abdullah:** Conceptualization, Writing - Review & Editing.

Declaration of competing interest

The authors clarify that there is no conflict of interest for report.

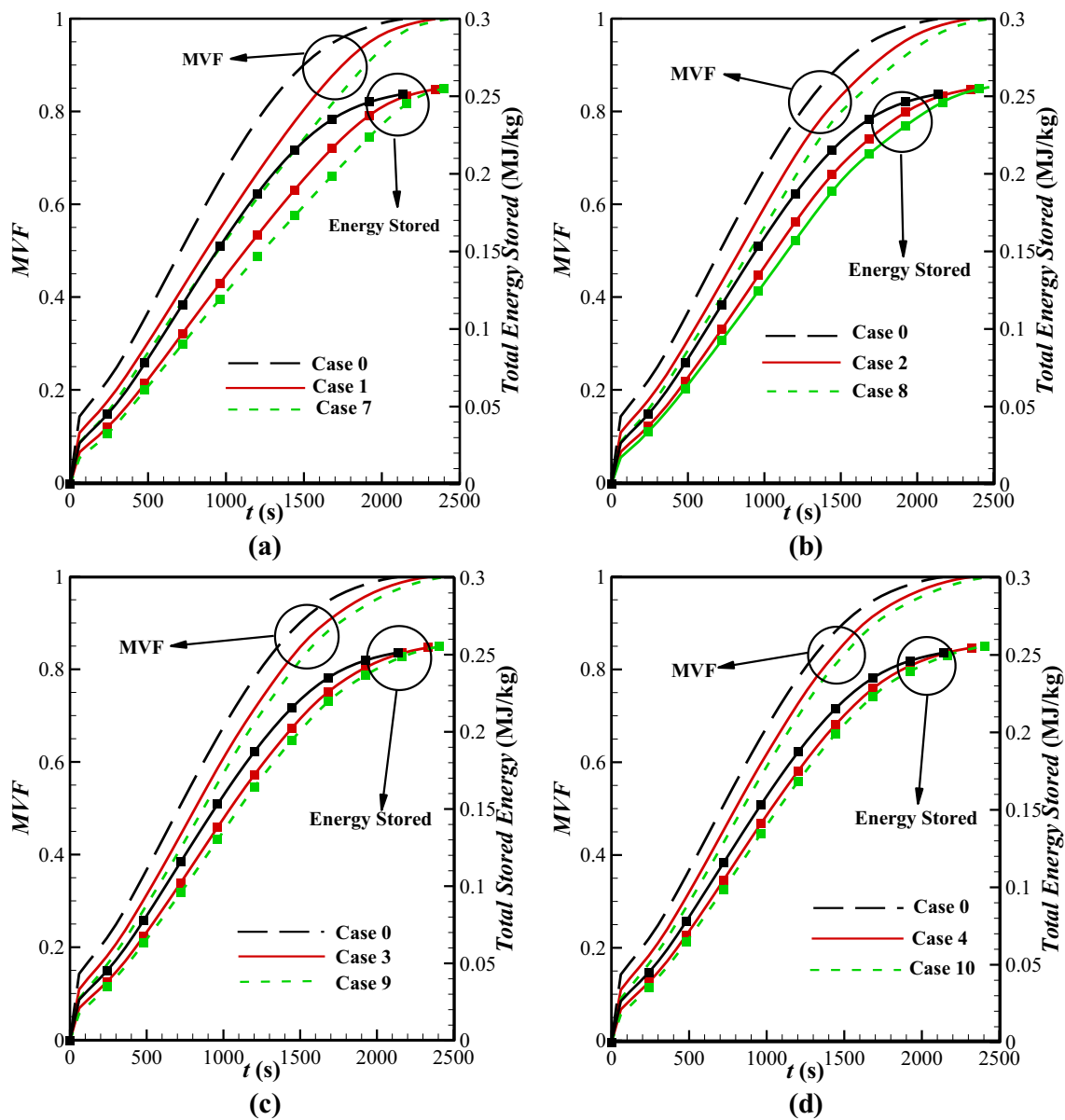


Fig. 11. Effect of wave amplitude on the melting volume fraction and total energy stored for double cases; (a) Cases 1 and 7 with $N = 1$, (b) Cases 2 and 8 with $N = 2$, (c) Cases 3 and 9 with $N = 3$, and (d) Cases 4 and 10 with $N = 4$.

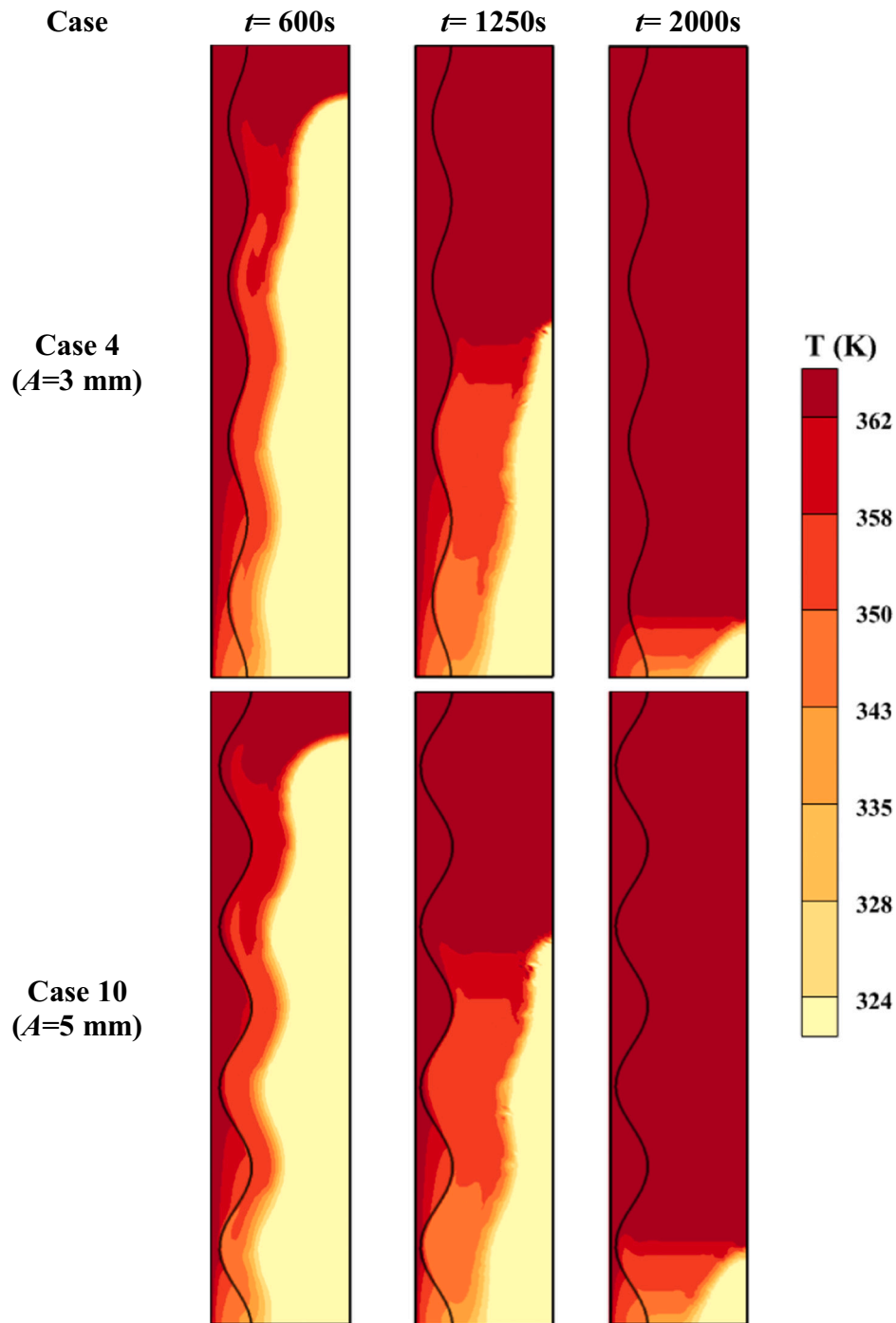


Fig. 12. Effect of the wave amplitude on the contours of isotherm; (Top row) Case 4 with $A = 3$ mm, and (Bottom row) Case 10 with $A = 5$ mm when $N = 4$. An increase in wave amplitude extends the metal foam into the enclosure more deeply. The presence of a foam layer boosts the conduction heat transfer and increases the temperature of the enclosure next to the foam edge.

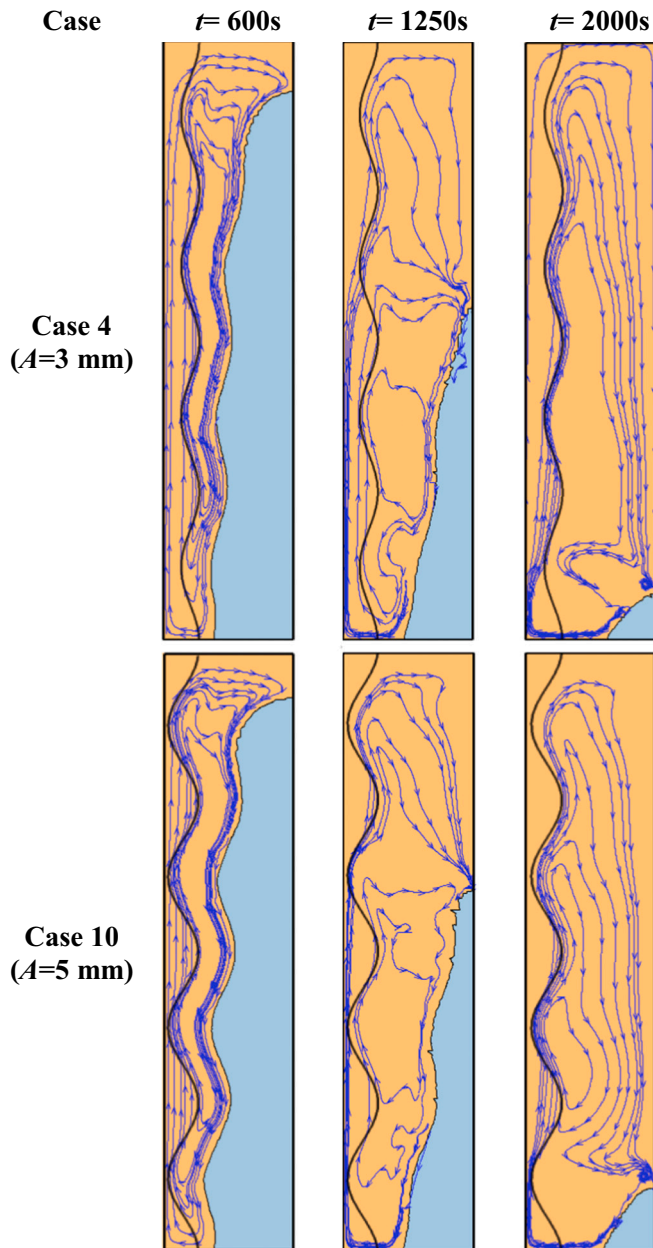


Fig. 13. Effect of the wave amplitude on the streamlines; (Top row) case 4 with $A = 3$ mm, and (Bottom row) Case 10 with $A = 5$ mm for $N = 4$. For a metal foam with a high amplitude of waviness, the depth of interface undulations is higher. The impact of waviness on the melting interface is pronounced at early times when the melting front is still close to the metal foam.

Data availability statements

All data generated or analyzed during this study are included in this published article.

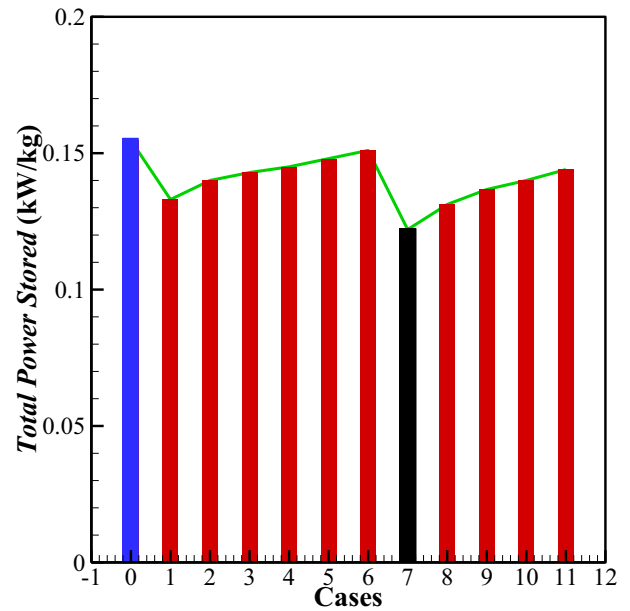


Fig. 14. Total energy storage power at $t = 1250$ s. The highest power rate corresponds to the case flat foam layer (case C0) followed by C6 with $A = 3$ and $N = 6$. The minimum power rate was produced by case C7 with an amplitude of $A = 5$ mm and $N = 1$.

Acknowledgment

The authors extend their appreciation to the Deputyship for Research & Innovation, Ministry of Education in Saudi Arabia for funding this research work through the project number (IF-PSAU-2021/01/18928).

References

- [1] X. Yu, J. Luan, W. Chen, J. Tao, Preparation and characterization of paraffin microencapsulated phase change material with double shell for thermal energy storage, *Thermochim. Acta* 689 (2020).
- [2] J. Lei, Y. Tian, D. Zhou, W. Ye, Y. Huang, Y. Zhang, Heat transfer enhancement in latent heat thermal energy storage using copper foams with varying porosity, *Sol. Energy* 221 (2021) 75–86.
- [3] T.-U. Rehman, T. Ambreen, H. Niyas, P. Kanti, H.M. Ali, C.-W. Park, Experimental investigation on the performance of RT-44HC-nickel foam-based heat sinks for thermal management of electronic gadgets, *Int. J. Heat Mass Transf.* 188 (2022).
- [4] S. Zhang, D. Feng, L. Shi, L. Wang, Y. Jin, L. Tian, Z. Li, G. Wang, L. Zhao, Y. Yan, A review of phase change heat transfer in shape-stabilized phase change materials (ss-PCMs) based on porous supports for thermal energy storage, *Renew. Sust. Energ. Rev.* 135 (2021).
- [5] R. Chaturvedi, A. Islam, K. Sharma, A review on the applications of PCM in thermal storage of solar energy, *Mater.TodayProc.* 43 (2021) 293–297.
- [6] W.T. Yan, C. Li, W.B. Ye, Numerical investigation of hydrodynamic and heat transfer performances of nanofluids in a fractal microchannel heat sink, *Heat Transf. Asian Res.* 48 (2019) 2329–2349.
- [7] W.T. Yan, W.B. Ye, C. Li, Effect of aspect ratio on saturated boiling flow in microchannels with nonuniform heat flux, *Heat Transf. Asian Res.* 48 (2019) 3312–3327.
- [8] N.B. Khedher, J.M. Mahdi, H.S. Majidi, W.K. Al-Azzawi, S. Dhahbi, P. Talebizadehsardari, A hybrid solidification enhancement in a latent-heat storage system with nanoparticles, porous foam, and fin-aided foam strips, *J. Energy Storage* 56 (2022), 106070.
- [9] Q. Li, C. Li, Z. Du, F. Jiang, Y. Ding, A review of performance investigation and enhancement of shell and tube thermal energy storage device containing molten salt based phase change materials for medium and high temperature applications, *Appl. Energy* 255 (2019).

- [10] B. Nie, A. Palacios, B. Zou, J. Liu, T. Zhang, Y. Li, Review on phase change materials for cold thermal energy storage applications, *Renew. Sust. Energ. Rev.* 134 (2020).
- [11] S. Wijesuriya, P.C. Tabares-Velasco, Empirical validation and comparison of methodologies to simulate micro and macro-encapsulated PCMs in the building envelope, *Appl. Therm. Eng.* 188 (2021).
- [12] M.H. Rostami, G. Najafi, A. Motevalli, N.A. Che Sidik, M.A. Harun, Evaluation and improvement of thermal energy of heat exchangers with SWCNT, GQD nanoparticles and PCM (RT82), *J.Adv.Res.Fluid Mech.Therm.Sci.* 79 (2020) 153–168.
- [13] M.E. Nakhchi, J.A. Esfahani, Improving the melting performance of PCM thermal energy storage with novel stepped fins, *J.Energy Storage* 30 (2020).
- [14] N. Aslfattahi, A. Zendejboudi, S. Rahman, M.F. Mohd Sabri, S. Mohd Said, A. Arifuzzaman, N.A. Che Sidik, Optimization of thermal conductivity of nanoPCM-based graphene by response surface methodology, *J.Adv.Res.Fluid Mech.Therm.Sci.* 75 (2020) 108–125.
- [15] M. Liu, Y. Sun, F. Bruno, A review of numerical modelling of high-temperature phase change material composites for solar thermal energy storage, *J.Energy Storage* 29 (2020).
- [16] C.Y. Zhao, Y.B. Tao, Y.S. Yu, Molecular dynamics simulation of nanoparticle effect on melting enthalpy of paraffin phase change material, *Int. J. Heat Mass Transf.* 150 (2020).
- [17] J. Guo, Z. Liu, Z. Du, J. Yu, X. Yang, J. Yan, Effect of fin-metal foam structure on thermal energy storage: an experimental study, *Renew. Energy* 172 (2021) 57–70.
- [18] W.Q. Li, S.J. Guo, L. Tan, L.L. Liu, W. Ao, Heat transfer enhancement of nano-encapsulated phase change material (NEPCM) using metal foam for thermal energy storage, *Int. J. Heat Mass Transf.* 166 (2021).
- [19] C. Ding, L. Wang, Z. Niu, Thermal performance evaluation of latent heat storage systems with plate fin-metal foam hybrid structure, *Case Stud.Therm.Eng.* 27 (2021).
- [20] S.N.J.Ercan Mehmet DEDE, Thermal Management Systems Including Multiple Phase Changing Materials And Vehicles Including the Same Vol. US20200136209A1, Toyota Motor Engineering & Manufacturing North America, Inc., Plano, TX (US), United States, 2018.
- [21] S.K. Razack, in: Khateeb Razack, Siddique Ali (Eds.), *Thermal Management System And Device*, European Patent Office, 2020.
- [22] W.-B. Ye, Finite volume analysis the thermal behavior of electrode non-uniformity, *Heat Mass Transf.* 53 (2017) 1123–1132.
- [23] P.T. Sardari, H.I. Mohammed, D. Giddings, G.S. Walker, M. Gillott, D. Grant, Numerical study of a multiple-segment metal foam-PCM latent heat storage unit: effect of porosity, pore density and location of heat source, *Energy* 189 (2019).
- [24] X. Li, Z. Zhu, Z. Xu, T. Ma, H. Zhang, J. Liu, X. Wang, Q. Wang, A three-dimensional pore-scale lattice Boltzmann model for investigating the supergravity effects on charging process, *Appl. Energy* 254 (2019).
- [25] I. Al Siyabi, S. Khanna, T. Mallick, S. Sundaram, An experimental and numerical study on the effect of inclination angle of phase change materials thermal energy storage system, *J.Energy Storage* 23 (2019) 57–68.
- [26] B.M.S. Punniakodi, R. Senthil, A review on container geometry and orientations of phase change materials for solar thermal systems, *J.Energy Storage* 36 (2021).
- [27] X. Yang, Z. Guo, Y. Liu, L. Jin, Y.-L. He, Effect of inclination on the thermal response of composite phase change materials for thermal energy storage, *Appl. Energy* 238 (2019) 22–33.
- [28] X. Yang, P. Wei, X. Cui, L. Jin, Y.-L. He, Thermal response of annuli filled with metal foam for thermal energy storage: an experimental study, *Appl. Energy* 250 (2019) 1457–1467.
- [29] Y. Yao, H. Wu, Thermal transport process of metal foam/paraffin composite (MFPC) with solid-liquid phase change: an experimental study, *Appl. Therm. Eng.* 179 (2020).
- [30] X. Meng, L. Yan, J. Xu, F. He, H. Yu, M. Zhang, Effect of porosity and pore density of copper foam on thermal performance of the paraffin-copper foam composite phase-change material, *Case Stud.Therm.Eng.* 22 (2020).
- [31] X. Meng, L. Yan, F. He, Filling copper foam partly on thermal behavior of phase-change material in a rectangular enclosure, *J.Energy Storage* 32 (2020).
- [32] S.M. Borhani, M.J. Hosseini, R. Pakrouh, A.A. Ranjbar, A. Nourian, Performance enhancement of a thermoelectric harvester with a PCM/metal foam composite, *Renew. Energy* 168 (2021) 1122–1140.
- [33] S. Huang, J. Lu, Y. Li, Numerical study on the influence of inclination angle on the melting behaviour of metal foam-PCM latent heat storage units, *Energy* 239 (2022).
- [34] X.K. Yu, Y.B. Tao, Y. He, Z.C. Lv, Temperature control performance of high thermal conductivity metal foam/paraffin composite phase change material: an experimental study, *J.Energy Storage* 46 (2022).
- [35] H.M. Ali, Heat transfer augmentation of porous media (metallic foam) and phase change material based heat sink with variable heat generations: an experimental evaluation, *Sustain.Energy Technol.Assess.* 52 (2022).
- [36] C. Ding, C. Zhang, L. Ma, A. Sharma, Numerical investigation on melting behaviour of phase change materials/metal foam composites under hypergravity conditions, *Appl. Therm. Eng.* 207 (2022).
- [37] N.A. Qasem, A. Abderrahmane, S. Ahmed, O. Younis, K. Guedri, Z. Said, A. Mourad, Effect of a rotating cylinder on convective flow, heat and entropy production of a 3D wavy enclosure filled by a phase change material, *Appl. Therm. Eng.* 214 (2022), 118818.
- [38] S. Singh, B.S. Negi, Numerical thermal performance investigation of phase change material integrated wavy finned single pass solar air heater, *J.Energy Storage* 32 (2020), 102002.
- [39] M. Eisapour, A.H. Eisapour, A. Shafaghat, H.I. Mohammed, P. Talebizadehsardari, Z. Chen, Solidification of a nano-enhanced phase change material (NePCM) in a double elliptical latent heat storage unit with wavy inner tubes, *Sol. Energy* 241 (2022) 39–53.
- [40] Y. Hong, J. Du, S. Wang, W.-B. Ye, S.-M. Huang, Turbulent thermal-hydraulic and thermodynamic characteristics in a traverse corrugated tube fitted with twin and triple wire coils, *Int. J. Heat Mass Transf.* 130 (2019) 483–495.
- [41] A. Parida, A. Bhattacharya, P. Rath, Effect of convection on melting characteristics of phase change material-metal foam composite thermal energy storage system, *J. Energy Storage* 32 (2020).
- [42] V. Joshi, M.K. Rathod, Thermal transport augmentation in latent heat thermal energy storage system by partially filled metal foam: a novel configuration, *J. Energy Storage* 22 (2019) 270–282.
- [43] A. Bhattacharya, V.V. Calmidi, R.L. Mahajan, Thermophysical properties of high porosity metal foams, *Int. J. Heat Mass Transf.* 45 (2002) 1017–1031.
- [44] X. Xiao, P. Zhang, M. Li, Preparation and thermal characterization of paraffin/metal foam composite phase change material, *Appl. Energy* 112 (2013) 1357–1366.
- [45] D.A. Nield, A. Bejan, *Convection in Porous Media*, Springer, 2006.
- [46] H. Zheng, C. Wang, Q. Liu, Z. Tian, X. Fan, Thermal performance of copper foam/paraffin composite phase change material, *Energy Convers. Manag.* 157 (2018) 372–381.
- [47] O.C. Zienkiewicz, R.L. Taylor, P. Nithiarasu, *The Finite Element Method for Fluid Dynamics*, Seventh Edition, Butterworth-Heinemann, Oxford, 2014.
- [48] G. Söderlind, L. Wang, Adaptive time-stepping and computational stability, *J. Comput. Appl. Math.* 185 (2006) 225–243.
- [49] B. Kamkari, H. Shokouhmand, F. Bruno, Experimental investigation of the effect of inclination angle on convection-driven melting of phase change material in a rectangular enclosure, *Int. J. Heat Mass Transf.* 72 (2014) 186–200.